Article

Ecological Performance Optimization of a High Temperature Proton Exchange Membrane Fuel Cell

Dongxu Li, Siwei Li, Zheshu Ma *, Bing Xu, Zhanghao Lu, Yanju Li and Meng Zheng

College of Automobile and Traffic Engineering, Nanjing Forestry University, Nanjing 210037, China;
Ldx961203@163.com (D.L.); wesly.li@outlook.com (S.L.); xb18260078388@163.com (B.X.);
L18252038553@163.com (Z.L.); njfulyj@163.com (Y.L.); mengzai19950929@163.com (M.Z.)
* Correspondence: mazheshu@njfu.edu.cn; Tel.: +86-137-7665-9269

Abstract: According to finite-time thermodynamics, an irreversible high temperature proton exchange membrane fuel cell (HT-PEMFC) model is established, and the mathematical expressions of the output power, energy efficiency, exergy efficiency and ecological coefficient of performance (ECOP) of HT-PEMFC are deduced. The ECOP is a step forward in optimizing the relationship between power and power dissipation, which is more in line with the principle of ecology. Based on the established HT-PEMFC model, the maximum power density is obtained under different parameters that include operating temperature, operating pressure, phosphoric acid doping level and relative humidity. At the same time, the energy efficiency, exergy efficiency and ECOP corresponding to the maximum power density are acquired so as to determine the optimal value of each index under the maximum power density. The results show that the higher the operating temperature and the doping level, the better the performance of HT-PEMFC is. However, the increase of operating pressure and relative humidity has little effect on HT-PEMFC performance.

Keywords: high temperature proton exchange membrane fuel cell; exergy analysis; ecological analysis; ecological coefficient of performance

1. Introduction

In recent years, proton exchange membrane fuel cells (PEMFCs) have been considered efficient and clean energy conversion devices. PEMFCs have been widely used in home equipment and automobiles [1] due to the advantage of higher power density, lower emission and noise. According to the operating temperature, PEMFC can be divided into low temperature proton exchange membrane fuel cell (70–95 °C) and high temperature proton exchange membrane fuel cell (120–200 °C). HT-PEMFC has the superiority of the accelerated kinetics of electrode reaction [2], higher CO tolerance [3], and simpler water and heat management systems [4,5].

At present, the research on HT-PEMFC mainly includes materials [6–8] and preparation methods [9,10]. Few people have used the first and second laws of thermodynamics to analyze and optimize the performance of HT-PEMFC. However, thermodynamic analysis and optimization of LT-PEMFC have been mature. Miansari et al. [11], Ozen et al. [12] and Esfeh et al. [13] verified that the operating temperature has a significant effect on the performance improvement of PEMFC. Li et al. [14,15] established the finite-time thermodynamic model of irreversible PEMFC, which considered polarization loss and leakage current. The effects of operating temperature, operating pressure and proton exchange membrane water content on the optimal performance of the irreversible proton exchange membrane fuel cell were numerically studied. Wei et al. [16] took the entropy production rate and ecological coefficient of performance of PEMFC as the objective function for numerical analysis, while optimal current density ranges were determined by different optimization objectives. Midilli et al. [17] found that higher current density and proton film thickness leads to a decrease in exergy efficiency of PEMFC. If the film thickness was the same, the exergy

efficiency of PEMFC is improved with the increase of operating pressure and the decrease of current density. Xu et al. [18] investigated exergetic sustainability indicators (ESI) of PEMFC under different parameters. Increasing the operating temperature and pressure decreases the irreversibility of PEMFC and increases exergetic sustainability indicators.

Therefore, the study of parameters based on thermodynamics is very important to boost the performance of PEMFC [11–23], thus, it has been applied to the irreversibility analysis and optimization of HT-PEMFC. Barati et al. [24] studied the influence of air and hydrogen flow rate, operating temperature and doping level of phosphoric acid on HT-PEMFC performance. The doping level has a significant effect on the performance improvement, mainly because the doping level of the membrane affected the proton conductivity of the membrane.

Lu et al. [25] established a mathematical model of HT-PEMFC and analyzed the exergy performance of the HT-PEMFC power generation system. Consequently, an improved farmland fertility optimization design method was put forward for optimizing the exergy, irreversibility and output power. Compared with the original design method and genetic algorithm, the number of iterations in the improved method was less, optimization speed was faster, and the output power density increased by 5.2 and 2.9%, respectively.

Xia et al. [26] investigated the effects of catalyst layer thickness, operating temperature, and proton exchange membrane thickness on HT-PEMFC performance. The results showed that the operating temperature has a significant effect on the performance. Operating temperature at 160–180 °C not only ensured the fuel cell performance, but also reduced maintenance costs at high temperatures. The thinner thickness of the catalyst layer and proton exchange membrane had a positive influence on the performance of HT-PEMFC, but it was easily damaged.

Guo et al. [19] analyzed the energetic, exergetic and ecological performance of HT-PEMFC and mathematical models of power density, entropy production rate and ecological coefficient of performance were established based on finite time thermodynamics theory. The results showed that the operating temperature and doping level have significant effects on the performance of HT-PEMFC. According to the optimization criterion of maximum power density, the optimization interval of current density is found to be the left of the current density corresponding to the maximum power density.
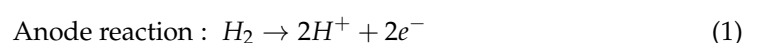
Lin et al. [27] investigated the exergy efficiency of HT-PEMFC using the meta-heuristic technique, and an improved collective animal behavior algorithm was utilized to evaluate and optimize the thermodynamic irreversibility, exergy efficiency and output power. Compared with the standard collective animal behavior algorithm and genetic algorithm, the proposed improved collective animal behavior algorithm increased the output power density by 1.2 and 12.1% and the exergy efficiency increased by 22.9%.

In this paper, firstly, a finite-time thermodynamic was introduced to analyze the irreversibility of HT-PEMFC, and a mathematical model which took irreversible losses and leakage current into consideration was established. Secondly, according to the maximum power density criterion, the optimization interval of current density was obtained and the optimal output efficiency, exergy efficiency and ecological coefficient of performance corresponding to the maximum power density were achieved. At the same time, the effects of operating temperature, operating pressure, relative humidity and doping level on the performance of HT-PEMFC were studied.

2. Thermodynamic Model

2.1. Working Principle of HT-PEMFC

As shown in Figure 1, HT-PEMFC can directly convert the chemical energy containing hydrogen and oxygen into electrical energy and heat energy. The whole system mainly includes a cathode, an anode and electrolyte. The reaction of anode and cathode show as follows:
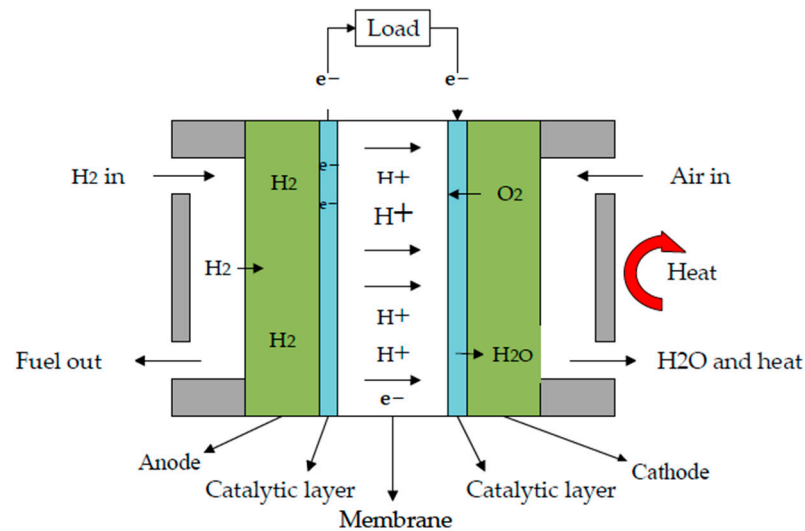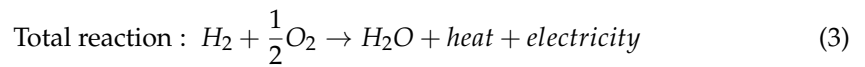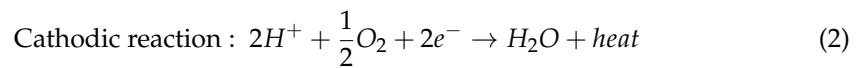
$$\text{Anode reaction}:\ H_2 \rightarrow 2H^+ + 2e^- \tag{1}$$

$$\text{Cathodic reaction}: \ 2H^+ + \frac{1}{2}O_2 + 2e^- \rightarrow H_2O + heat \tag{2}$$

$$\text{Total reaction}: \ H_2 + \frac{1}{2}O_2 \rightarrow H_2O + heat + electricity \tag{3}$$

Figure 1. Working principle of an HT-PEMFC system fueled with H_2 and O_2.

2.2. Reversible Potential of HT-PEMFC

For HT-PEMFC, reversible potential [28,29] shows as follows:

$$E_r = E_r^0 + \frac{\Delta S}{nF}(T - 298.15) + \frac{RT}{nF}\ln\left(\frac{p_{H_2}\,p_{O_2}^{0.5}}{p_{H_2O}}\right) \tag{4}$$

in Equation (4), E_r^0 is the ideal standard potential which value is 1.185 V, ΔS is the change of standard molar entropy, T is the operating temperature of HT-PEMFC, R is the gas constant, p_{H_2}, p_{O_2} and p_{H_2O} are partial pressures of H_2, O_2 and H_2O, respectively.

$$\frac{\Delta S}{n} = -18.449 - 0.01283 \cdot T \tag{5}$$

where ΔS is related to the operating temperature.

2.3. Overpotential of HT-PEMFC

For HT-PEMFC, due to three types of overpotential containing activation overpotential, concentration overpotential and ohmic overpotential, its actual output voltage is generally less than the reversible potential.

- Activation overpotential [29,30];

$$E_{act} = \frac{RT}{n\alpha F}\ln\left(\frac{j + j_{leak}}{j_0}\right) \tag{6}$$

$$\ln j_{leak} = \left(-2342.9\frac{1}{T} + 9.0877\right) \tag{7}$$

where α is charge transfer coefficient, j_{leak} is leakage current density, j_0 is exchange current density.

- Concentration overpotential [28];

$$E_{con} = \left(1 + \frac{1}{\alpha}\right) \frac{RT}{nF} \ln\left(\frac{j_L}{j_L - j}\right) \tag{8}$$

where j is operating current density, j_L is limiting current density [29].
- Ohmic overpotential [31];

$$E_{ohm} = j \frac{t_{mem}}{\sigma_{mem}} \tag{9}$$

where t_{mem} is the thickness of the electrolyte, σ_{mem} is the proton conductivity of the electrolyte [31].

$$\sigma_{mem} = \frac{A_0 B}{T} e^{\frac{-b_{act}}{RT}} \tag{10}$$

$$A_0 = 68DL^3 - 6324DL^2 + 65750DL + 8460 \tag{11}$$

$$B = \begin{cases} 1 + (0.01704T - 4.767)RH & 373.15K \leq T \leq 413.15 \\ 1 + (0.1432T - 56.89)RH & 413.15K < T \leq 453.15 \\ 1 + (0.7T - 309.2)RH & 453.15 < T \leq 473.15 \end{cases} \tag{12}$$

$$b_{act} = -619.6DL + 21750 \tag{13}$$

| noindent where DL is the doping level of the electrolyte, RH is the relative humidity of the electrolyte [29].
- Output voltage;

According to Equations (1)–(13), the output voltage [32] of the HT-PEMFC can be derived as follows:

$$U = E_{rev} - E_{con} - E_{act} - E_{ohm} = E_{rev} - \left(1 + \frac{1}{\alpha}\right) \frac{RT}{nF} \ln\left(\frac{j_L}{j_L - j}\right) - \frac{RT}{n\alpha F} \ln\left(\frac{j + j_{leak}}{j_0}\right) - j \frac{t_{mem}}{\sigma_{mem}} \tag{14}$$

2.4. Finite-Time Thermodynamic Performance Analysis of HT-PEMFC

All analyses are based on the following assumptions:

1. With the HT-PEMFC system operating in a quasi-steady state, provided that the operating temperature and operating pressure are continuously changing, it is assumed that the operating pressure and operating temperature are constant at a fixed time;
2. The enthalpy of hydrogen entering the HT-PEMFC determines the maximum working capacity of the HT-PEMFC;
3. The exergy [33] mainly contains chemical exergy ε_{chem} and physical exergy ε_{phy}, the kinetic and potential exergy of the hydrogen are neglected

$$\varepsilon = \varepsilon_{chem} + \varepsilon_{phy} \tag{15}$$

4. The energy required for compressing reactants is ignored.

- Output power density [34];

The output power density of the HT-PEMFC can be expressed as follows:

$$P = jU \tag{16}$$

- Output efficiency [35];

For any energy conversion device, the thermal efficiency is the energy output divided by the total energy input. Therefore, the output efficiency of HT-PEMFC can be shown as Equation (16):

$$\eta = \frac{P}{-\Delta \dot{H}} \tag{17}$$

where $\Delta\dot{H}$ is the total energy absorbed from hydrogen and oxygen.

$$\Delta\dot{H} = -\frac{jA\Delta h}{nF} \tag{18}$$

where Δh is the change of molar enthalpy.

- Exergy efficiency [36,37];

Exergy is an indicator used to evaluate energy quality. Exergy efficiency of HT-PEMFC, φ, is defined as the utilization degree of exergy, can be represented by:

$$\varphi = \frac{PA}{\dot{\varepsilon}_{in}} \tag{19}$$

$$\dot{\varepsilon}_{in} = \frac{jA}{nF}\left(\varepsilon_{H_2} + 0.5\varepsilon_{O_2}\right) \tag{20}$$

where $\dot{\varepsilon}_{in}$ is the total input exergy rate of H_2 and O_2; A is the electrode effective surface area; ε_{H_2} and ε_{O_2} are the standard chemical exergy of H_2 and O_2.

- Ecological coefficient of performance [14,23];

In addition to energetic and exergetic analyses, the energy conversion performance of HT-PEMFC can also be analyzed by ecological standards. Angulo [38] proposed the ecological criterion function $E = P - T_L\dot{\delta}$ based on the heat engine, where P is output power, $T_L\dot{\delta}$ reflects the power dissipation of the engine. The objective function not only optimizes the output power, but also takes the power dissipation into account, which makes the objective conform to the principle of long-term ecology. On this basis, Ust [39,40] presented a new ecological objective function, known as the ecological coefficient of performance (ECOP), which is the ratio of output power to power dissipation. Compared with the previous ecological objective function, the relationship between output power and power dissipation is improved. Its expression is as follows:

$$ECOP = \frac{PA}{T_0\dot{\delta}} \tag{21}$$

$$\dot{\delta} = \frac{-\Delta\dot{H} - P}{T} \tag{22}$$

2.5. Finite-Time Thermodynamic Optimization of HT-PEMFC

Since the output power and output efficiency of HT-PEMFC cannot reach the maximum at the same time, in order to minimize the power consumption of HT-PEMFC, the maximum output power is taken as the optimization objective. The power density of HT-PEMFC first increases and then decreases with the continuous increase of current density. Therefore, within a certain minimum range of current density, the power density of HT-PEMFC is bound to reach the maximum.

The power density of HT-PEMFC is related to current density j, operating temperature T, operating pressure p, relative humidity RH and phosphoric acid doping level DL, which can be written as

$$P = f(j, T, p, RH, DL) \tag{23}$$

When p, RH and DL are constant, the power density is only related to current density and operating temperature, which can be presented as

$$P_1 = h(j, T) \tag{24}$$

When the operating temperature of HT-PEMFC is T_1, the power is only related to current density j, and the maximum power density is obtained, and the corresponding

current density is j_1. Therefore, the maximum output power density at the operating temperature T_1 can be shown as

$$P_{1,max}^* = \max g(j) \tag{25}$$

By analogy, when the operating temperature of HT-PEMFC is T_n, the maximum power density is $P_{n,max}^*$, and the corresponding current density is j_n. Thus, the relationship between the maximum output power density $P_{n,max}^*$ of HT-PEMFC and operating temperature T_n is deduced. In addition, similar methods can be used to study the influence of operating pressure, doping level and relative humidity on the maximum output power density of HT-PEMFC. The relationship between these parameters and the maximum output power density can also be acquired, which can further boost the power density of HT-PEMFC.

2.6. Output Efficiency, Exergy Efficiency and ECOP Based on Maximum Output Power Density

During the operation of HT-PEMFC, the output efficiency η decreases with the increase of current density j. Therefore, the output efficiency reaches the maximum value in the low current density region, but the power density is low. In order to ensure the lowest power dissipation of HT-PEMFC, the current density j_n, corresponding to the maximum power density, is obtained according to the optimization criterion of the maximum power density. Thus, the output efficiency of HT-PEMFC corresponding to j_n is the most efficient. In order to further improve the performance of HT-PEMFC, the effects of operating temperature, operating pressure, relative humidity and doping level on the output efficiency of HT-PEMFC are studied, and the relationship between these parameters and output efficiency is obtained.

As can be seen from the curve of exergy efficiency φ and ecological coefficient of performance coefficient $ECOP$ of HT-PEMFC, with the continuous work of HT-PEMFC, φ and $ECOP$ decrease with the increase of current density. Therefore, the method of obtaining the relationship between φ and $ECOP$ and different parameters is similar to that of obtaining the relationship between output efficiency and different parameters.

2.7. Comparsion of Optimization Analysis of Different Objective Functions

Different objective functions include the maximum output power density $\overline{P}$, the optimal output efficiency $\overline{\eta}$ at the maximum output power density, the optimal exergy efficiency $\overline{\phi}$ at the maximum output power density and ecological coefficient of performance $\overline{ECOP}$ at the maximum output power density, where $\overline{P}$, $\overline{\eta}$, $\overline{\phi}$ and $\overline{ECOP}$ are dimensionless functions [41]. The dimensionless maximum output power density of HT-PEMFC can be expressed as follows:

$$\overline{P} = \frac{P_{max}}{P_{2,max}} \tag{26}$$

where P_{max} is the maximum output power density of HT-PEMFC at different operating temperature, and $P_{2,max}$ is the maximum output power density of HT-PEMFC at the operating pressure $p = 2\ atm$. The dimensionless method of output efficiency, exergy efficiency and ecological coefficient of performance corresponding to the maximum power density is similar to that of the dimensionless maximum power density.

3. Results and Discussion

3.1. Model Verification

Figure 2 compares the predicted model voltage and the experimental data [42] of HT-PEMFC at 423 K and 448 K (p = 1 atm; DL = 5.6; RH = 0.38%), the experimental data are in good agreement with the predicted data. Figure 3 shows the relationship between reversible potential (E_{rev}), concentration overpotential (E_{con}), activation overpotential (E_{act}), ohmic overpotential (E_{ohm}), and output voltage (U) with current density. The reversible potential is a constant independent of current density. The three kinds of over-potential increase with the increase of current density, the concentration overpotential increases exponentially, the activation overpotential grows logarithmically, and the ohmic overpotential grows less.

In the low current density region, the rapid decline of output voltage is mainly due to the rapid increase of activation overpotential. In the region of high current density, the output voltage drops rapidly, mainly because the concentration overpotential increases rapidly.
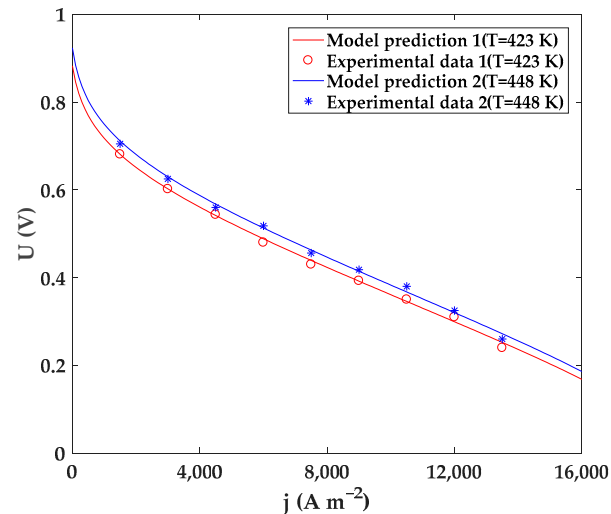

Figure 2. Comparisons of the predicted model voltage and experimental data.
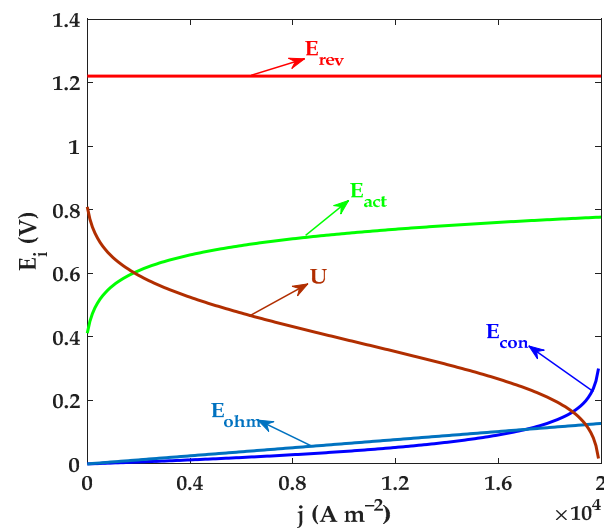

Figure 3. The relationship between reversible potential, concentration overpotential, activation overpotential, ohmic overpotential and current density.

3.2. Influences of the Operating Temperature

Figure 4a shows the variation of the dimensionless maximum power density of HT-PEMFC with operating temperature under different pressure. It can be seen that the maximum power density of the irreversible HT-PEMFC improves continuously with the increase of operating temperature. This is mainly because, as the operating temperature rises, the exchange current density grows, so the activation overpotential decreases. At the same time, the increase of operating temperature will enhance the proton conductivity, which will reduce the ohmic overpotential of HT-PEMFC. Therefore, the power loss produced by ohmic overpotential and activation overpotential will be cut down. Therefore, as the growth of operating temperature, the maximum power density of HT-PEMFC will increase constantly. When the operating pressure is 1 atm and the operating temperature is 403 K, the corresponding maximum power density is 3071.58 W m^{-2}. When the operating temperature rises up to 473 K, the corresponding maximum power density is 5291.60 W m^{-2}.

This indicates that the maximum power density of HT-PEMFC increases by 72%, when the operating temperature of HT-PEMFC increases from 403 K to 473 K. The maximum power density increases by 70% and 73%, respectively, at 2 atm and 3 atm. The result shows that HT-PEMFC can significantly increase its maximum power density in a suitable operating temperature range.
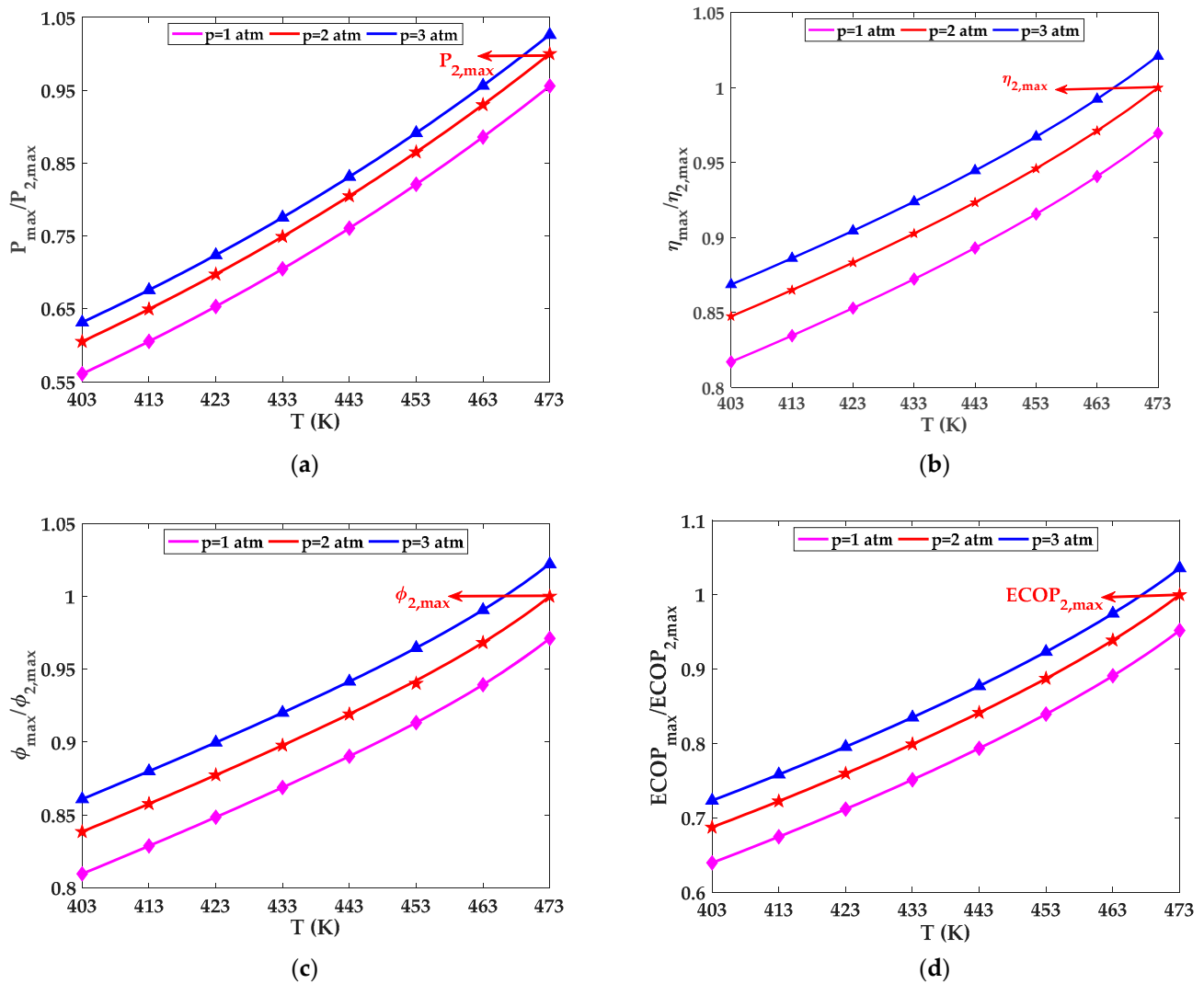

Figure 4. (**a**) $\overline{P}$ varying with operating temperature; (**b**) $\overline{\eta}$ varying with operating temperature; (**c**) $\overline{\phi}$ varying with operating temperature; (**d**) $\overline{ECOP}$ varying with operating temperature.

Figure 4b–d reflect the $\overline{\eta}$, $\overline{\phi}$ and $\overline{ECOP}$ corresponding to the maximum power density of HT-PEMFC. It is obvious that the increase of operating temperature can improve the output efficiency, exergy efficiency and ECOP of the irreversible process of HT-PEMFC. When the operating pressure is 1 atm and the operating temperature is 403 K, the corresponding output efficiency is 22.3%, exergy efficiency is 25.93% and ECOP is 37.23%. When the operating temperature is 473 K, the corresponding output efficiency is 26.46%, exergy efficiency is 31.3%, and ECOP is 55.97%. This shows that when the operating temperature of HT-PEMFC increased from 130 °C to 200 °C, its output efficiency, exergy efficiency and ECOP increased by 19, 21 and 50%, respectively. The increase of HT-PEMFC temperature accelerates the passage rate of protons and increases the conductivity of the proton exchange membrane, so the power generation of HT-PEMFC boosts, as well as the output efficiency and exergy efficiency. As the power consumption lessens, the entropy generated decreases and the output power increases, so the ratio of output power to power consump-

tion increases, that is, the ecological coefficient of performance ECOP improves. However, though raising the operating temperature can improve the performance of HT-PEMFC, it can also cause many problems, such as high cost, poor stability, and long start-up time.

3.3. Influences of the Operating Pressure

Figure 5a shows that $\overline{P}$ of HT-PEMFC changes with operating pressure at different operating temperatures. Obviously, with the increase of operating pressure, the maximum power density of irreversible HT-PEMFC is continuously increasing. Owing that as the exchange current density rises with the rise of the operating pressure, the activation overpotential will decrease and the reversible potential will boost. Therefore, with the increase of operating pressure, the irreversibility of HT-PEMFC decreases and the maximum power density of HT-PEMFC increases continuously. When the operating temperature is 453 K and the operating pressure is 1 atm, the corresponding maximum power density is 4515.13 W m^{-2}. When the operating pressure rises up to 3 atm, the corresponding maximum power density is 4919.07 W m^{-2}. From the numerical point of view, when the operating temperature is 453 K and the operating temperature of HT-PEMFC increases from 1 atm to 3 atm, the maximum power density of HT-PEMFC only increases by 9%. This shows that operating pressure has little influence on HT-PEMFC.
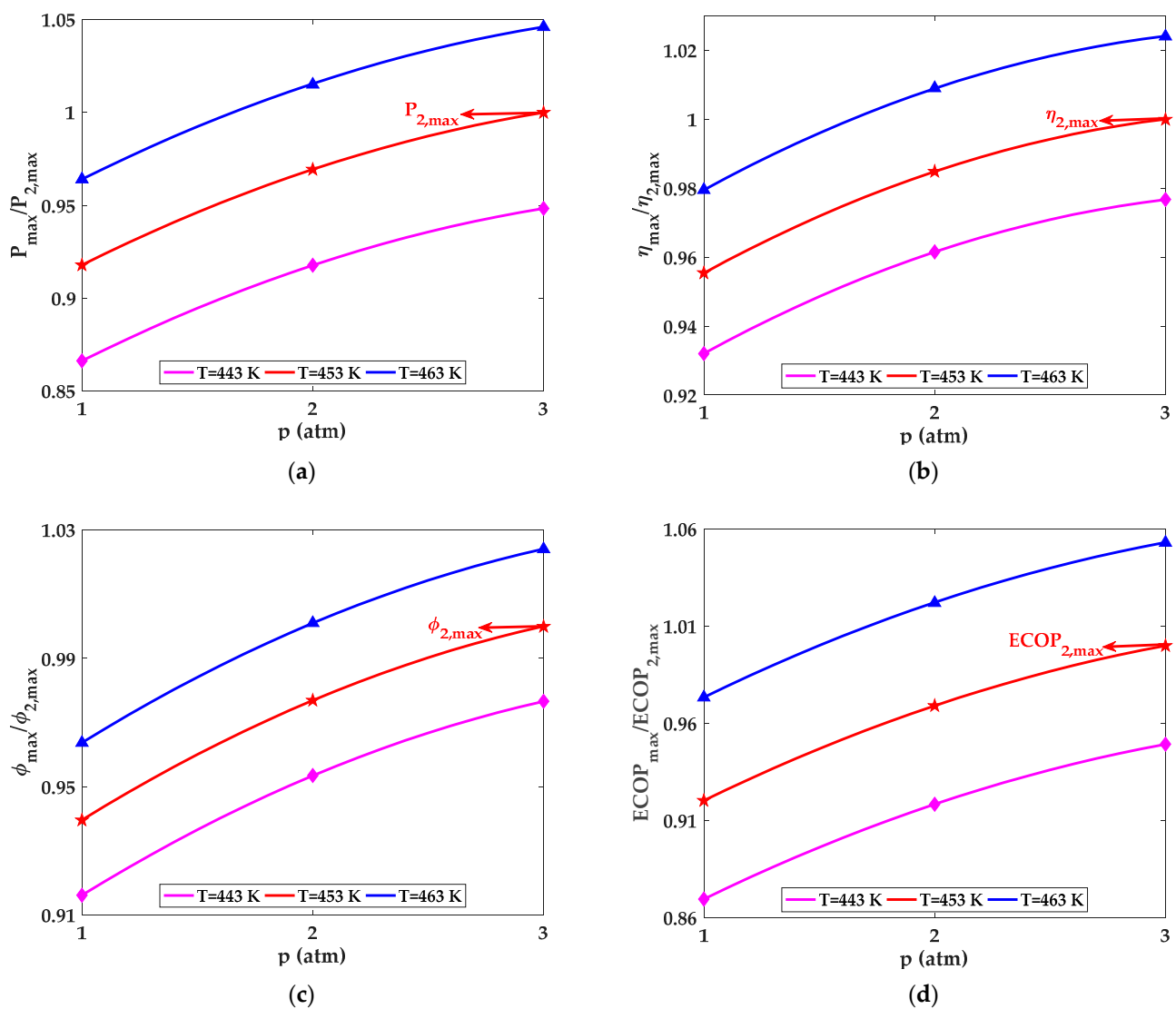
Figure 5. (**a**) $\overline{P}$ varying with operating pressure; (**b**) $\overline{\eta}$ varying with operating pressure; (**c**) $\overline{\phi}$ varying with operating pressure; (**d**) $\overline{ECOP}$ varying with operating pressure.

It can be seen from Figure 5b–d that $\overline{\eta}$, $\overline{\phi}$ and $\overline{ECOP}$ correspond to the maximum power density of HT-PEMFC. The increase of operating pressure can slightly improve the output efficiency, exergy efficiency and ECOP of the irreversible process of HT-PEMFC. When the operating temperature of HT-PEMFC increased from 1 atm to 3 atm, its output efficiency, exergy efficiency and ECOP increased by 5, 6 and 9%, respectively. According to the numerical analysis, the increase of operating pressure does not improve the performance of HT-PEMFC as significantly as the increase of operating temperature. In addition, increasing the operating pressure consumes extra power to compress the reactants in the inlet, resulting in higher costs.

3.4. Influences of the Doping Level

As shown in Figure 6, with the increase of current density, ohmic overpotential will improve. When doping level rises, the proton conductivity of HT-PEMFC increases, which reduces the ohmic overpotential. According to the relationship between $\overline{P}$ and DL in Figure 7a, it can be observed that the maximum power density raises endlessly with the increase of doping level. This is mainly because, as the rise of doping level, the ohmic overpotential decreases and the reversible potential improves. Hence, if the doping level of HT-PEMFC is raised appropriately, the maximum power density will become larger. When the doping level is 2, the corresponding maximum power density is 1868.52 W m^{-2}. When the doping level is 10, the corresponding maximum power is 4694.53 W m^{-2}. It is clear that when the doping level increases from 2 to 10 and relative humidity is 3.8%, the maximum power density of HT-PEMFC increases by 150%. This indicates that DL has a significant effect on the performance of HT-PEMFC.
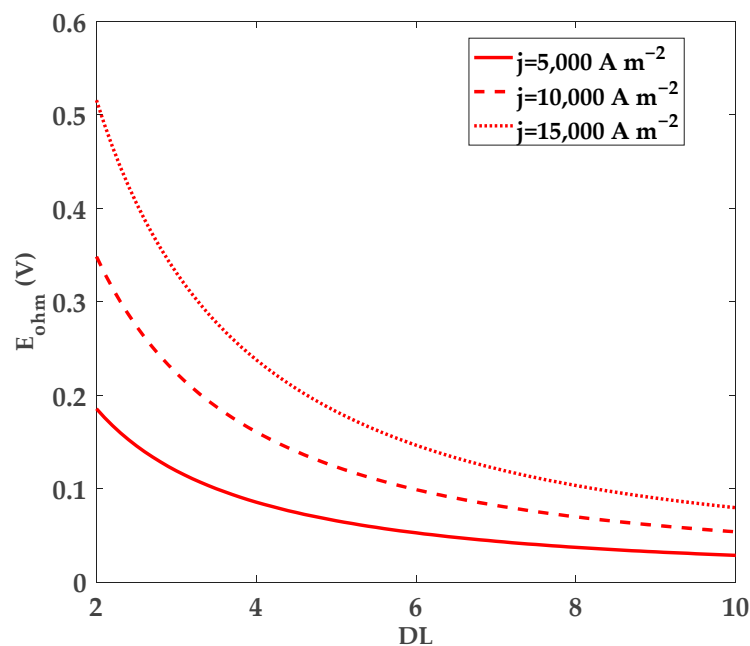

Figure 6. The relationship between ohmic overpotential and doping level at different current density (T = 453 K, p = 1 atm, RH = 3.8%).

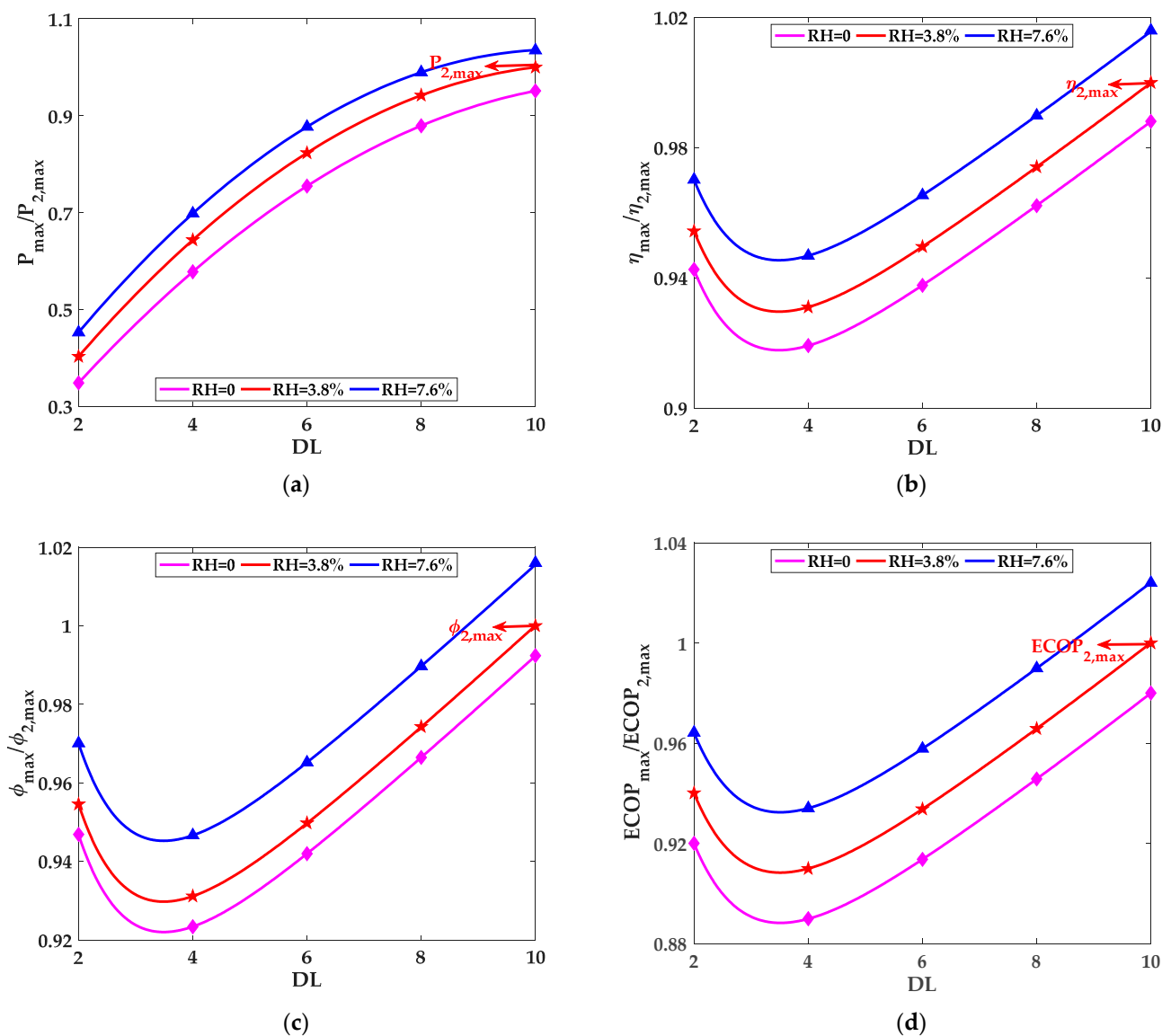**Figure 7.** (**a**) $\overline{P}$ varying with doping level; (**b**) $\overline{\eta}$ varying with doping level; (**c**) $\overline{\phi}$ varying with doping level; (**d**) $\overline{ECOP}$ varying with doping level.

Figure 7b–d show the $\overline{\eta}$, $\overline{\phi}$ and $\overline{ECOP}$ corresponding to the maximum power density of HT-PEMFC varying with doping level at different relative humidity. It can be seen that when the doping level increases, the output efficiency, exergy efficiency and ECOP of HT-PEMFC all showed a trend of decreasing at first and then increasing. This is mainly because the current density of the maximum is different under different doping levels. When the doping level is small, the current density is low and the gap of current density of the maximum power density at different doping levels is bigger, thus causing ohmic potential increases with the increase of DL. When the doping level is high, the current density corresponding to the maximum power density is in the region of high current density, and the difference of the current density of the maximum power density is small at different doping level, so the ohmic overpotential decreases with the increase of DL, leading to the increase of reversible potential. When the relative humidity of HT-PEMFC is 3.8% and the doping level increases from 2 to 10, its output efficiency, exergy efficiency and ECOP increases by 5, 5 and 6%, respectively. This indicates that doping level significantly improved the maximum power density, but has little impact on output efficiency, exergy efficiency and ECOP.

3.5. Influences of the Relative Humidity

Figure 8a shows the change of $\overline{P}$ with relative humidity at different temperatures. It can be seen that with the increase of relative humidity, the maximum power density of irreversible HT-PEMFC rises. The main reason is that with the increase of relative humidity, the conductivity of the proton exchange membrane at high temperature will boost, resulting in the decrease of ohmic overpotential. When RH is 0, the corresponding maximum power density is 4064.78 W m^{-2}. When RH rises up to 7.6%, the corresponding maximum power density is 4168.1 W m^{-2}. This indicates that the maximum power density of HT-PEMFC increases by only 2% when the operating temperature is 453 K and the relative humidity increases from 0 to 7.6%. As shown in Figure 9, although relative humidity can improve proton conductivity, increasing relative humidity has less effect on the ohmic overpotential than the doping level. Therefore, relative humidity has little effect on the maximum power density of HT-PEMFC.
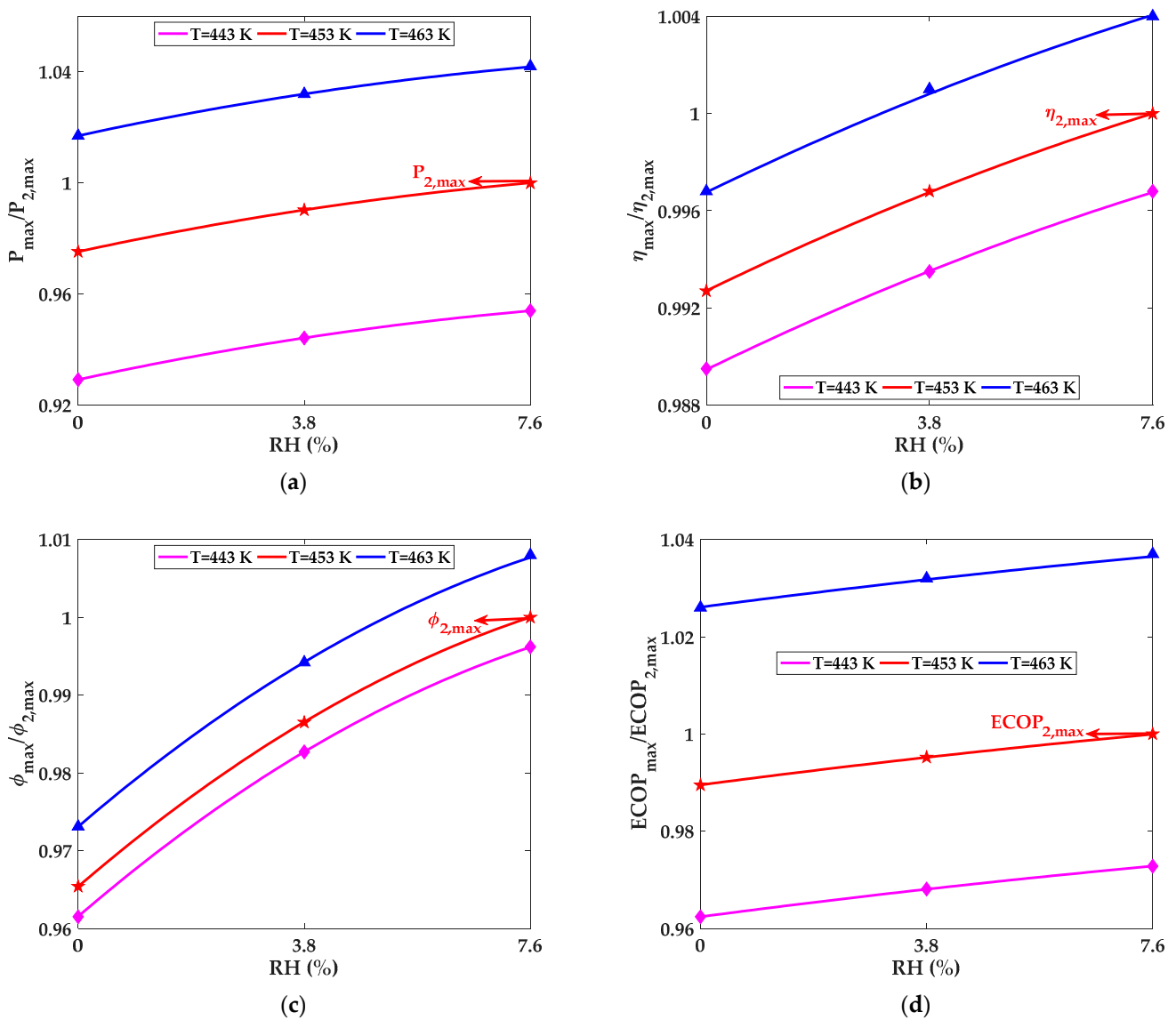

Figure 8. (**a**) $\overline{P}$ varying with relative humidity; (**b**) $\overline{\eta}$ varying with relative humidity; (**c**) $\overline{\phi}$ varying with relative humidity; (**d**) $\overline{ECOP}$ varying with relative humidity.
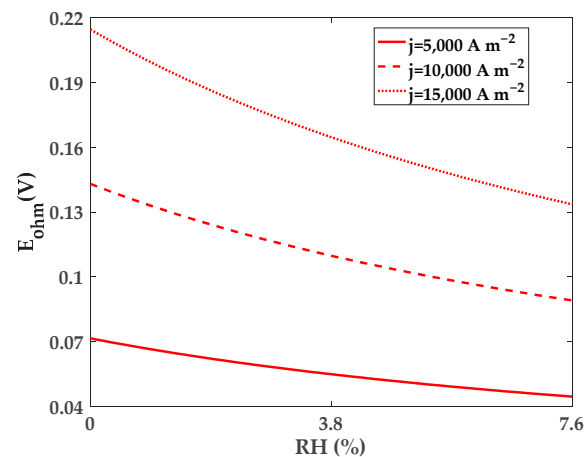
Figure 9. The relationship between ohmic overpotential and relative humidity at different current density (T = 453 K, p = 1 atm, DL = 8).

Figure 8b–d reflect $\overline{\eta}$, $\overline{\phi}$ and $\overline{ECOP}$ corresponding to the maximum power density of HT-PEMFC varying with relative humidity at different temperatures. It can be seen from the figures that the three indexes all show a monotonically increasing trend. When the relative humidity is 0 and the operating temperature is 453 K, the corresponding output efficiency is 24.5%, exergy efficiency was 25.1%, and ECOP is 48.16%. When the relative humidity was 7.6%, the corresponding output efficiency was 24.68%, exergy efficiency was 26%, and ECOP was 48.667%. It reflects that when the relative humidity of HT-PEMFC increased from 0 to 7.6%, its output efficiency, exergy efficiency and ECOP increased by 0.7, 4 and 1%, respectively. Compared with the consequences of doping levels, the numerical results of relative humidity are significantly lower. Therefore, relative humidity has little effect on the performance improvement of HT-PEMFC.

4. Conclusions

In this paper, the irreversibility caused by polarization and leakage current is considered, and the finite-time thermodynamic model of HT-PEMFC is established. The influence of operating temperature, operating pressure, doping level of phosphoric acid and relative humidity on the maximum output power density is studied. In addition, according to the maximum power density criterion, the influence of different parameters on output efficiency, exergy efficiency and ecological coefficient of performance is obtained. Among them, ECOP compromises the relationship between power and efficiency performance of HT-PEMFC.

Through numerical analysis and calculation, when the operating temperature increases from 403 K to 473 K, the maximum output power density increases by 72%, the output efficiency rises by 19%, the exergy efficiency rises by 21%, and the ecological performance coefficient boosts by 50%. When the doping level of phosphoric acid increases from 2 to 10, the maximum power density increases by 150%. However, the operating pressure and relative humidity have little influence on the maximum power density and the output efficiency, exergy efficiency and ECOP.

In the future, the extended irreversible thermodynamics [43,44] that expands the scope of classical irreversible thermodynamics into a new field could be considered to analyze the HT-PEMFC system.

Author Contributions: All of the authors contributed to publishing this article. The collection of materials and summarization of this article was done by D.L. and Y.L. The simulation and analysis were done by Z.L., S.L. and M.Z. The conceptual ideas, methodology and guidance for the research were provided by Z.M. and B.X. All authors have read and agreed to the published version of the manuscript.

Institutional Review Board Statement: Not applicable.

Informed Consent Statement: Not applicable.

Data Availability Statement: Not applicable.

Conflicts of Interest: The authors declare no conflict of interest.

References

1. Haider, R.; Wen, Y.; Ma, Z.-F.; Wilkinson, D.P.; Zhang, L.; Yuan, X.; Song, S.; Zhang, J. High temperature proton exchange membrane fuel cells: Progress in advanced materials and key technologies. *Chem. Soc. Rev.* **2021**, *50*, 1138–1187. [CrossRef] [PubMed]
2. Devrim, Y.; Arıca, E.D. Multi-walled carbon nanotubes decorated by platinum catalyst for high temperature PEM fuel cell. *Int. J. Hydrog. Energy* **2019**, *44*, 18951–18966. [CrossRef]
3. Alpaydin, G.U.; Devrim, Y.; Colpan, C.O. Performance of an HT-PEMFC having a catalyst with graphene and multiwalled carbon nanotube support. *Int. J. Energy Res.* **2019**, *43*, 3578–3589. [CrossRef]
4. Nalbant, Y.; Colpan, C.O.; Devrim, Y. Energy and exergy performance assessments of a high temperature-proton exchange membrane fuel cell based integrated cogeneration system. *Int. J. Hydrog. Energy* **2020**, *45*, 3584–3594. [CrossRef]
5. Reddy, E.H.; Jayanti, S. Thermal management strategies for a 1 kWe stack of a high temperature proton exchange membrane fuel cell. *Appl. Therm. Eng.* **2012**, *48*, 465–475. [CrossRef]
6. Lee, D.; Lim, J.W.; Gil Lee, D. Cathode/anode integrated composite bipolar plate for high-temperature PEMFC. *Compos. Struct.* **2017**, *167*, 144–151. [CrossRef]
7. Oono, Y.; Sounai, A.; Hori, M. Influence of the phosphoric acid-doping level in a polybenzimidazole membrane on the cell performance of high-temperature proton exchange membrane fuel cells. *J. Power Sources* **2009**, *189*, 943–949. [CrossRef]
8. Pinar, F.J.; Cañizares, P.; Rodrigo, M.A.; Úbeda, D.; Lobato, J. Long-term testing of a high-temperature proton exchange membrane fuel cell short stack operated with improved polybenzimidazole-based composite membranes. *J. Power Sources* **2015**, *274*, 177–185. [CrossRef]
9. Li, Q.; Rudbeck, H.; Chromik, A.; Jensen, J.; Pan, C.; Steenberg, T.; Calverley, M.; Bjerrum, N.J.; Kerres, J. Properties, degradation and high temperature fuel cell test of different types of PBI and PBI blend membranes. *J. Membr. Sci.* **2010**, *347*, 260–270. [CrossRef]
10. Muthuraja, P.; Prakash, S.; Shanmugam, V.; Radhakrsihnan, S.; Manisankar, P. Novel perovskite structured calcium titanate-PBI composite membranes for high-temperature PEM fuel cells: Synthesis and characterizations. *Int. J. Hydrog. Energy* **2018**, *43*, 4763–4772. [CrossRef]
11. Miansari, M.; Sedighi, K.; Amidpour, M.; Alizadeh, E. Experimental and thermodynamic approach on proton exchange membrane fuel cell performance. *J. Power Sources* **2009**, *190*, 356–361. [CrossRef]
12. Ozen, D.N.; Timurkutluk, B.; Altinisik, K. Effects of operation temperature and reactant gas humidity levels on performance of PEM fuel cells. *Renew. Sustain. Energy Rev.* **2016**, *59*, 1298–1306. [CrossRef]
13. Esfeh, H.K.; Hamid, M.K.A. Temperature Effect on Proton Exchange Membrane Fuel Cell Performance Part II: Parametric Study. *Energy Procedia* **2014**, *61*, 2617–2620. [CrossRef]
14. Li, C.; Liu, Y.; Xu, B.; Ma, Z. Finite Time Thermodynamic Optimization of an Irreversible Proton Exchange Membrane Fuel Cell for Vehicle Use. *Processes* **2019**, *7*, 419. [CrossRef]
15. Li, C.J.; Liu, Y.; Ma, Z.S. Thermodynamic Analysis of the Performance of an Irreversible PEMFC. *Defect Diffus. Forum* **2018**, *388*, 350–360. [CrossRef]
16. Wei, F.F.; Huang, Y.W. Performance Characteristics of an Irreversible Proton Exchange Membrane (PEM) Fuel Cell. *J. Donghua Univ.* **2012**, *29*, 393–398.
17. Ay, M.; Midilli, A.; Dincer, I. Exergetic performance analysis of a PEM fuel cell. *Int. J. Energy Res.* **2005**, *30*, 307–321. [CrossRef]
18. Xu, B.; Chen, Y.; Ma, Z.S. Exergetic sustainability indicators of a polymer electrolyte membrane fuel cell at variable operating conditions. *Arch. Thermodyn.* **2021**, *42*, 183–204.
19. Guo, Y.; Guo, X.; Zhang, H.; Hou, S. Energetic, exergetic and ecological analyses of a high-temperature proton exchange membrane fuel cell based on a phosphoric-acid-doped polybenzimidazole membrane. *Sustain. Energy Technol. Assess.* **2020**, *38*, 100671. [CrossRef]
20. Haghighi, M.; Sharifhassan, F. Exergy analysis and optimization of a high temperature proton exchange membrane fuel cell using genetic algorithm. *Case Stud. Therm. Eng.* **2016**, *8*, 207–217. [CrossRef]
21. Ishihara, A.; Mitsushima, S.; Kamiya, N.; Ota, K.-I. Exergy analysis of polymer electrolyte fuel cell systems using methanol. *J. Power Sources* **2004**, *126*, 34–40. [CrossRef]
22. Xie, D.; Wang, Z.; Jin, L.; Zhang, Y. Energy and exergy analysis of a fuel cell based micro combined heat and power cogeneration system. *Energy Build.* **2012**, *50*, 266–272. [CrossRef]

23. Li, C.; Xu, B.; Ma, Z. Ecological Performance of an Irreversible Proton Exchange Membrane Fuel Cell. *Sci. Adv. Mater.* **2020**, *12*, 1225–1235. [CrossRef]
24. Barati, S.; Ghazi, M.M.; Khoshandam, B. Study of effective parameters for the polarization characterization of PEMFCs sensitivity analysis and numerical simulation. *Korean J. Chem. Eng.* **2018**, *36*, 146–156. [CrossRef]
25. Lu, X.; Li, B.; Guo, L.; Wang, P.; Yousefi, N. Exergy analysis of a polymer fuel cell and identification of its optimum operating conditions using improved Farmland Fertility Optimization. *Energy* **2021**, *216*, 119264. [CrossRef]
26. Xia, L.; Zhang, C.; Hu, M.; Jiang, S.; Chin, C.S.; Gao, Z.; Liao, Q. Investigation of parameter effects on the performance of high-temperature PEM fuel cell. *Int. J. Hydrog. Energy* **2018**, *43*, 23441–23449. [CrossRef]
27. Lin, D.; Han, Y.H.; Khodaei, H. Application of the meta-heuristics for optimizing exergy of a HT-PEMFC. *Int. J. Energ. Res.* **2020**, *44*, 3749–3761. [CrossRef]
28. Guo, X.; Zhang, H.; Zhao, J.; Wang, F.; Wang, J.; Miao, H.; Yuan, J. Performance evaluation of an integrated high-temperature proton exchange membrane fuel cell and absorption cycle system for power and heating/cooling cogeneration. *Energy Convers. Manag.* **2019**, *181*, 292–301. [CrossRef]
29. Lee, W.-Y.; Kim, M.; Sohn, Y.-J.; Kim, S.-G. Power optimization of a combined power system consisting of a high-temperature polymer electrolyte fuel cell and an organic Rankine cycle system. *Energy* **2016**, *113*, 1062–1070. [CrossRef]
30. Cheddie, D.; Munroe, N. Analytical correlations for intermediate temperature PEM fuel cells. *J. Power Sources* **2006**, *160*, 299–304. [CrossRef]
31. Olapade, P.O.; Meyers, J.P.; Borup, R.L.; Mukundan, R. Parametric Study of the Morphological Proprieties of HT-PEMFC Components for Effective Membrane Hydration. *J. Electrochem. Soc.* **2011**, *158*, B639–B649. [CrossRef]
32. Mamaghani, A.H.; Najafi, B.; Casalegno, A.; Rinaldi, F. Optimization of an HT-PEM fuel cell based residential micro combined heat and power system: A multi-objective approach. *J. Clean. Prod.* **2018**, *180*, 126–138. [CrossRef]
33. Al-Sulaiman, F.A.; Dincer, I.; Hamdullahpur, F. Exergy analysis of an integrated solid oxide fuel cell and organic Rankine cycle for cooling, heating and power production. *J. Power Sources* **2010**, *195*, 2346–2354. [CrossRef]
34. Wu, Z.; Zhu, P.; Yao, J.; Tan, P.; Xu, H.; Chen, B.; Yang, F.; Zhang, Z.; Ni, M. Thermo-economic modeling and analysis of an NG-fueled SOFC-WGS-TSA-PEMFC hybrid energy conversion system for stationary electricity power generation. *Energy* **2020**, *192*, 116613. [CrossRef]
35. Zhang, X.; Cai, L.; Liao, T.; Zhou, Y.; Zhao, Y.; Chen, J. Exploiting the waste heat from an alkaline fuel cell via electrochemical cycles. *Energy* **2018**, *142*, 983–990. [CrossRef]
36. Cohce, M.; Dincer, I.; Rosen, M. Energy and exergy analyses of a biomass-based hydrogen production system. *Bioresour. Technol.* **2011**, *102*, 8466–8474. [CrossRef]
37. Nguyen, H.Q.; Aris, A.M.; Shabani, B. PEM fuel cell heat recovery for preheating inlet air in standalone solar-hydrogen systems for telecommunication applications: An exergy analysis. *Int. J. Hydrog. Energy* **2016**, *41*, 2987–3003. [CrossRef]
38. Angulo-Brown, F. An ecological optimization criterion for finite-time heat engines. *J. Appl. Phys.* **1991**, *69*, 7465–7469. [CrossRef]
39. Ust, Y.; Sahin, B.; Sogut, O.S. Performance analysis and optimization of an irreversible dual-cycle based on an ecological coefficient of performance criterion. *Appl. Energy* **2005**, *82*, 23–39. [CrossRef]
40. Ust, Y.; Sahin, B.; Kodal, A. Performance analysis of an irreversible Brayton heat engine based on ecological coefficient of performance criterion. *Int. J. Therm. Sci.* **2006**, *45*, 94–101. [CrossRef]
41. E, Q.; Wu, F.; Chen, L.-G.; Qiu, Y.-N. Thermodynamic optimization for a quantum thermoacoustic refrigeration micro-cycle. *J. Cent. South. Univ.* **2020**, *27*, 2754–2762. [CrossRef]
42. Sousa, T.; Mamlouk, M.; Scott, K. An isothermal model of a laboratory intermediate temperature fuel cell using PBI doped phosphoric acid membranes. *Chem. Eng. Sci.* **2010**, *65*, 2513–2530. [CrossRef]
43. Chen, K.C.; Yeh, C.S. Extended Irreversible Thermodynamics Approach to Magnetorheological Fluids. *J. Non-Equilib. Thermodyn.* **2001**, *26*, 355–372. [CrossRef]
44. Versaci, M.; Palumbo, A. Magnetorheological Fluids: Qualitative comparison between a mixture model in the Extended Irreversible Thermodynamics framework and an Herschel–Bulkley experimental elastoviscoplastic model. *Int. J. Non-Linear Mech.* **2020**, *118*, 103288. [CrossRef]